

Radiative corrections in $K \rightarrow \pi \ell^+ \ell^-$ decays

Bastian Kubis, Rebekka Schmidt

Helmholtz-Institut für Strahlen- und Kernphysik (Theorie) and Bethe Center for Theoretical Physics, Universität Bonn, D-53115 Bonn, Germany

Abstract. We calculate radiative corrections to the flavor-changing neutral current process $K \rightarrow \pi \ell^+ \ell^-$, both for charged and neutral kaon decays. While the soft-photon approximation is shown to work well for the muon channels, we discuss the necessity of further phase space cuts with electrons in the final state. It is also shown how to transfer our results to other decays such as $\eta \rightarrow \gamma \ell^+ \ell^-$ or $\omega \rightarrow \pi^0 \ell^+ \ell^-$.

PACS. 13.20.Eb Decays of K mesons – 13.25.Jx Decays of other mesons – 13.40.Ks Electromagnetic corrections to strong- and weak-interaction processes

1 Introduction

The radiative non-leptonic decay $K \rightarrow \pi \ell^+ \ell^-$ ($\ell = e, \mu$) offers insight into the nature of the weak interactions at low energies. These flavor-changing neutral current transitions are suppressed to the one-loop level in the standard model, where the CP-allowed channels $K^\pm \rightarrow \pi^\pm \ell^+ \ell^-$ and $K_S \rightarrow \pi^0 \ell^+ \ell^-$ are expected to be dominated by one-photon exchange ($K \rightarrow \pi \gamma^*$). The real-photon decay $K \rightarrow \pi \gamma$ is forbidden by gauge invariance, and in the effective-theory description of chiral perturbation theory, also the virtual transition is suppressed to the one-loop level [1]. $K \rightarrow \pi \ell^+ \ell^-$ has since been investigated in chiral perturbation theory beyond one-loop order [2, 3] and with isospin breaking included [4].

The least rare of these decays, $K^\pm \rightarrow \pi^\pm e^+ e^-$, the first to be discovered at the CERN PS [5] and subsequently studied with increasing precision at BNL [6], has now been investigated by the modern high-precision experiments E865 in Brookhaven [7] and NA48/2 at CERN [8], both with numbers of events of the order of 10^4 . For the muon decay channel $K^\pm \rightarrow \pi^\pm \mu^+ \mu^-$, a few hundred events have been recorded at BNL [9, 10] and Fermilab [11], and NA48/2 is in the process of analyzing a sample of ~ 3000 events [12]; the K_S decays have been seen by NA48/1, though with a handful of events only so far [13, 14]. As a welcome side effect of the upcoming NA62 experiment dedicated to the search of the very rare $K \rightarrow \pi \nu \bar{\nu}$ decays, a strong future increase in statistics for $K \rightarrow \pi \ell^+ \ell^-$ is also expected, making the availability of reliable (electromagnetic) radiative corrections an indispensable requirement.

As the chiral representation of the $K \rightarrow \pi \gamma^*$ form factor starts at the one-loop level, a full analysis of radiative corrections in the framework of chiral perturbation theory seems highly impractical, as it would require a two-loop calculation already at leading non-trivial order. Fur-

thermore, the counterterms appearing in such processes (weak non-leptonic with electromagnetic corrections at two loops) have never been considered, let alone the finite parts of such counterterms estimated phenomenologically. We therefore follow a more pragmatic approach akin to the study of soft-photon corrections in meson decays in Ref. [15] and restrict ourselves largely to universal radiative corrections, assuming a linear form factor; in this way, a technically simpler one-loop calculation suffices. Given that the data are still compatible with such a linear form factor approximation [7, 8], this seems a reasonable procedure. Furthermore, as the only non-analyticity in the form factor occurring within the physical decay region is the $\pi^+ \pi^-$ intermediate state that necessarily has to appear in a P-wave [2], the deviation from an analytic behavior is moderate, with the corresponding imaginary part rising slowly above the $\pi\pi$ threshold.

We shall see below, after introducing the necessary formalism in Sect. 2, that for the most interesting corrections concerning the invariant mass spectrum of the lepton–antilepton pair, the assumption of a specific form factor is actually not of high concern, as it factorizes neatly. These results are contained in Sect. 3. We discuss the soft-photon approximation for the bremsstrahlung, and how the appearance of collinear singularities for the electron–positron final state enforces to go beyond that, introducing additional phase space cuts. The form factor slope only affects those radiative corrections that induce an $\ell^+ \ell^-$ asymmetry, which we investigate in Sect. 4. Despite quite different hadronic currents contracted with the leptonic ones, we demonstrate in Sect. 5 that a significant part of our results can be transferred directly to other meson decays involving lepton–antilepton pairs in the final state, such as the Dalitz decays $\pi^0 \rightarrow \gamma e^+ e^-$, $\eta \rightarrow \gamma \ell^+ \ell^-$, or the vector meson conversion decays $\omega \rightarrow \pi^0 \ell^+ \ell^-$, $\phi \rightarrow \eta \ell^+ \ell^-$ etc. Finally, we conclude with a summary; several of the more laborious formulas are relegated to the appendices.

2 Formalism

We consider the decay $K(k) \rightarrow \pi(p) \ell^+(p_+) \ell^-(p_-)$ in terms of the kinematic variables $s = (k-p)^2$, $t = (k-p_+)^2$, $u = (k-p_-)^2$. For the CP-allowed (K^\pm and K_S) channels, the $K \rightarrow \pi \gamma^*$ form factor $F(s)$ is defined as

$$i \int d^4x e^{i(k-p)x} \langle \pi(p) | T \{ J_{\text{em}}^\mu(x) \mathcal{L}_{\Delta S=1}(0) \} | K(k) \rangle \\ = \frac{e F(s)}{M_K^2 (4\pi)^2} [s(k+p)^\mu - (k^2 - p^2)(k-p)^\mu] , \quad (1)$$

which on the kaon and pion mass shell simplifies according to $k^2 = M_K^2$, $p^2 = M_\pi^2$. Here, J_{em}^μ is the electromagnetic current and $\mathcal{L}_{\Delta S=1}$ the strangeness-changing non-leptonic weak Lagrangian. The form factors $F(s)$ are (potentially) very different for K^\pm and K_S decays [2]; for simplicity we refrain from reflecting this explicitly in the notation. Contracting Eq. (1) with the leptonic current yields the decay amplitude

$$\mathcal{M}(K \rightarrow \pi \ell^+ \ell^-) = -\frac{e^2 F(s)}{M_K^2 (4\pi)^2} \bar{u}(p_-) (\not{k} + \not{p}) v(p_+) , \quad (2)$$

which, when squared and summed over fermion spins, results in the Dalitz plot distribution

$$d\Gamma = \frac{\alpha^2 |F(s)|^2}{4(4\pi)^5 M_K^7} (\lambda - \nu^2) ds d\nu , \quad (3)$$

where $\alpha = e^2/4\pi$ is the fine structure constant, $\lambda \doteq \lambda(M_K^2, s, M_\pi^2)$ with the Källén function $\lambda(a, b, c) = a^2 + b^2 + c^2 - 2(ab + ac + bc)$, and $\nu = t - u$. Integrating over ν , with the limits of the Dalitz plot given by

$$-\nu_{\text{max}} \leq \nu \leq \nu_{\text{max}} , \quad \nu_{\text{max}} = \sigma \lambda^{1/2} , \quad \sigma = \sqrt{1 - \frac{4m^2}{s}} , \quad (4)$$

and m is the mass of the lepton involved, we find the spectrum with respect to the dilepton invariant mass as

$$\frac{d\Gamma}{ds} = \frac{\alpha^2 |F(s)|^2}{2(4\pi)^5 M_K^7} \lambda^{3/2} \sigma \left(1 - \frac{\sigma^2}{3}\right) . \quad (5)$$

Due to the Dirac structures in the leptonic current, radiative corrections in these decays cannot easily be written as one overall correction factor to the Dalitz plot distribution Eq. (3) (compare Ref. [15]). This is easily seen by the virtual-photon exchange between lepton and antilepton, see Fig. 1, which is precisely the diagram responsible for the generation of the anomalous magnetic moment at leading order, and hence a new Dirac structure. In general, we write the radiative corrections to the Dalitz plot in the form

$$d\Gamma = \frac{\alpha^2 |F(s)|^2}{4(4\pi)^5 M_K^7} \left[(\lambda - \nu^2)(1 + \omega + \hat{\omega}) + \nu^2 \bar{\omega} + m^2 \nu \tilde{\omega} \right] ds d\nu , \quad (6)$$

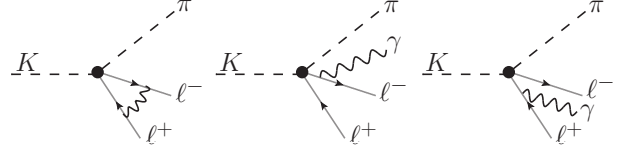


Fig. 1. Feynman graphs contributing to radiative corrections in $K_S \rightarrow \pi^0 \ell^+ \ell^-$ through virtual- and real-photon processes. We do not show diagrams responsible for (electromagnetic) wave function renormalization.

where ω , $\bar{\omega}$, and $\tilde{\omega}$ are even functions in ν , while $\hat{\omega}$ is odd; all four of them are of order α . This leads to a corrected dilepton spectrum according to

$$\frac{d\Gamma}{ds} = \frac{\alpha^2 |F(s)|^2}{2(4\pi)^5 M_K^7} \lambda^{3/2} \sigma \left(1 - \frac{\sigma^2}{3}\right) (1 + \Omega) , \\ \Omega = \omega + \frac{\sigma^2}{3 - \sigma^2} \bar{\omega} . \quad (7)$$

The relation between Ω , ω , and $\bar{\omega}$ in Eq. (7) will be implicitly assumed for all parts and approximations discussed for these correction factors in the following section. The factors $\hat{\omega}$ and $\tilde{\omega}$ (which are only non-vanishing for the *charged* kaon decay) cancel in $d\Gamma/ds$ upon integration of the terms odd in ν . They do, however, induce an asymmetry in ν (or $\ell^+ \ell^-$ asymmetry) to which, in turn, ω and $\bar{\omega}$ do not contribute. This asymmetry will be defined and discussed in Sect. 4. Finally, we remark that, in this article, we do not discuss effects due to vacuum polarization in the one-photon exchange graphs, which can simply be taken care of by the properly renormalized running fine structure constant α .

3 Radiative corrections for $d\Gamma/ds$

3.1 $K \rightarrow \pi \mu^+ \mu^-$: soft-photon approximation

It is well known that loop corrections involving massless particles (e.g., photons) diverge in the infrared. These divergences are exactly canceled by the contributions from real-photon emission (bremsstrahlung) [16–18], which is typically included up to some maximum photon energy E_{max} ; remnants of the infrared divergence can then be seen by terms depending logarithmically on E_{max} . The finite, not logarithmically enhanced terms depend on the choice of reference frame in which this cut is applied. While a conventional choice in decays is the rest frame of the decaying particle, we would like to argue that this is not very advantageous in the case at hand: as the predominant interest in this decay lies in the extraction of the form factor $F(s)$ from data, a preferred option is to use a cutoff in the rest frame of the $\ell^+ \ell^- \gamma$ system in the final state, or $\mathbf{k} - \mathbf{p} = 0$. In this way, the bremsstrahlung contribution—like the rest of the electromagnetic corrections—is essentially a function of s only and does not induce any $\ell^+ \ell^-$ asymmetry by itself. The results we present in the following always refer to this choice for the photon-energy cut.

E_{\max} is then given by the minimum of a cutoff energy E_{cut} and the kinematic limit,

$$E_{\max} = \min \left\{ E_{\text{cut}}, \frac{s - 4m^2}{2\sqrt{s}} \right\}. \quad (8)$$

The bremsstrahlung calculation is typically the hardest part of the radiative corrections at $\mathcal{O}(\alpha)$. It is drastically simplified in the so-called soft-photon approximation, which consists essentially in neglecting the photon momentum in the overall momentum-conserving δ -function; as a consequence, also all kinematic variables can be chosen identical to the non-radiative process. It is easy to show that the soft-photon approximation differs from the exact results by terms of order E_{\max} , i.e. reproduces the logarithmic terms as well as terms of order E_{\max}^0 correctly. With a typical cutoff of $E_{\text{cut}} = 20 \dots 30$ MeV, and a process such as $K \rightarrow \pi \mu^+ \mu^-$ in which all mass scales are significantly larger than E_{\max} , the soft-photon approximation is therefore expected to work very well. We shall verify this below.

There may actually be other processes contributing to real-photon emission besides bremsstrahlung, i.e. the radiation of a soft photon from one of the external charged particles, namely so-called structure-dependent contributions. These structure-dependent terms can be shown to also be of $\mathcal{O}(E_{\max})$, hence comparable to those neglected in the soft-photon approximation. In the process at hand, there is a very large structure-dependent contribution from $K^+ \rightarrow \pi^+ \pi^0$ with subsequent Dalitz decay $\pi^0 \rightarrow \gamma e^+ e^-$, which however occurs at fixed $s = M_{\pi^0}^2$. To avoid contamination with structure-dependent photon radiation, the cutoff E_{\max} may not be chosen too large. As a side remark, this should currently not be a major issue, as even the main (non-radiative) decay $K^+ \rightarrow \pi^+ e^+ e^-$ is only measured for $s > M_{\pi^0}^2$ to avoid background from $K^+ \rightarrow \pi^+ \pi^0$ with subsequent $\pi^0 \rightarrow e^+ e^-$.

We begin by discussing the simplest of the decay channels with respect to radiative corrections, $K_S \rightarrow \pi^0 \mu^+ \mu^-$. Obviously, photons can only couple to the charged leptons in the final state. The diagrams contributing to both virtual- and real-photon corrections are shown in Fig. 1. The resulting correction factors are given by $\omega(K_S \rightarrow \pi^0 \mu^+ \mu^-) = \omega_{\ell^+ \ell^-}^{\text{soft}}$ and correspondingly for $\bar{\omega}$ and Ω , where

$$\begin{aligned} \omega_{\ell^+ \ell^-}^{\text{soft}} &= \frac{\alpha}{\pi} \left\{ 2 \left(\frac{1 + \sigma^2}{2\sigma} \log \frac{1 + \sigma}{1 - \sigma} - 1 \right) \left(\log \frac{2E_{\max}}{m} + 1 \right) \right. \\ &\quad + \frac{1 + \sigma^2}{2\sigma} \left[\pi^2 - 2 \text{Li} \left(\frac{2\sigma}{\sigma + 1} \right) + 2 \text{Li} \left(\frac{2\sigma}{\sigma - 1} \right) \right] \\ &\quad \left. + \frac{\sigma}{2} \log \frac{1 + \sigma}{1 - \sigma} - \frac{1}{2} \right\}, \\ \bar{\omega}_{\ell^+ \ell^-}^{\text{soft}} &= -\frac{\alpha}{\pi} \frac{1 - \sigma^2}{2\sigma} \log \frac{1 + \sigma}{1 - \sigma}, \end{aligned} \quad (9)$$

where $\text{Li}(z)$ is the dilogarithm or Spence function,

$$\text{Li}(z) = - \int_0^z \frac{\log(1-t)}{t} dt. \quad (10)$$

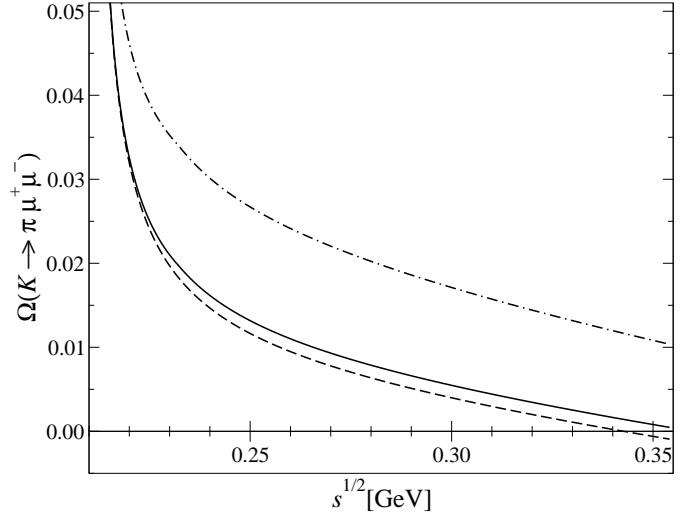


Fig. 2. Correction factor for $d\Gamma/ds(K_S \rightarrow \pi^0 \mu^+ \mu^-)$, both in soft-photon approximation (full line) and for the exact result (dashed), plus the correction factor for $d\Gamma/ds(K^+ \rightarrow \pi^+ \mu^+ \mu^-)$ in soft-photon approximation (dash-dotted curve). All terms are given for a photon-energy cutoff $E_{\text{cut}} = 20$ MeV.

The expressions in Eq. (9) are ultraviolet finite and do not require a counterterm; this is a consequence of the Ward identity in QED. The resulting correction factor $\Omega_{\ell^+ \ell^-}^{\text{soft}}$ is plotted in Fig. 2. At small s , it is obviously dominated by the Coulomb pole in Eq. (9),

$$\Omega_{\ell^+ \ell^-}^{\text{C}} = \frac{\alpha}{\pi} \frac{1 + \sigma^2}{2\sigma} \pi^2, \quad (11)$$

which is the leading approximation (in α) to the Gamow–Sommerfeld factor [19, 20]. Next-to-leading order corrections (of $\mathcal{O}(\alpha^2)$) become important as soon as $\alpha(1 + \sigma^2)/2\sigma$ is not small any more, which, in the present case of muons involved, happens in the sub-keV region above threshold. Given the expected energy resolution of kaon decay experiments, the approximation Eq. (11) is therefore surely sufficient.

The exact expression $\Omega_{\ell^+ \ell^-}$, without the soft-photon approximation, is given in Appendix A. For illustration, we compare exact and soft-photon form for $E_{\text{cut}} = 20$ MeV in Fig. 2: the differences are small, of the order of 0.2% at most. This is in accordance with a corresponding comparison for radiative corrections in $K \rightarrow 3\pi$ decays [21] (which has rather similar kinematics to $K \rightarrow \pi \mu^+ \mu^-$). Changing the cutoff to $E_{\text{cut}} = 30$ MeV hardly changes the picture.

The generalization to the correction factor $\Omega(K^+ \rightarrow \pi^+ \mu^+ \mu^-)$ for the dilepton spectrum is surprisingly simple. It is given as

$$\Omega(K^+ \rightarrow \pi^+ \mu^+ \mu^-) = \Omega_{\ell^+ \ell^-} + \Omega_{K\pi}, \quad (12)$$

where $\Omega_{K\pi}$ is calculated exclusively from the diagrams displayed in Fig. 3, i.e. those graphs that would also constitute the radiative corrections in $K^+ \rightarrow \pi^+ \nu \bar{\nu}$, say. All virtual-photon corrections linking mesons and leptons, or

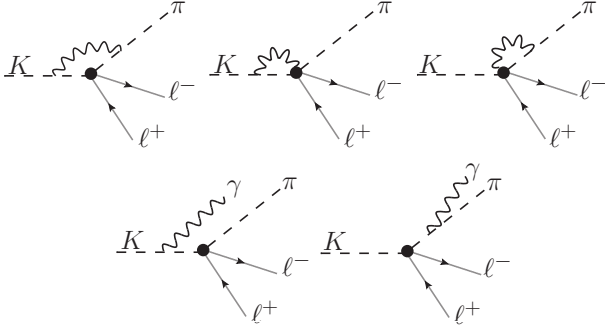


Fig. 3. Additional Feynman graphs contributing to radiative corrections in $d\Gamma/ds(K^+ \rightarrow \pi^+ \ell^+ \ell^-)$ through virtual (top) and real (bottom) photon processes. Again, diagrams contributing to wave function renormalization are not shown explicitly.

the interference of meson and lepton bremsstrahlung, are odd in $t - u$ and hence cancel in the dilepton spectrum (they are part of the correction factors $\hat{\omega}$ and $\tilde{\omega}$ to be discussed in Sect. 4). Furthermore, $\Omega_{K\pi} = \omega_{K\pi}$, as obviously radiative corrections only concerning the hadronic current do not induce a new Dirac structure, $\tilde{\omega}_{K\pi} = 0$. We only calculate $\omega_{K\pi}$ in the soft-photon approximation, for which we find the analytic representation

$$\begin{aligned} \omega_{K\pi}^{\text{soft}} = & \frac{\alpha}{\pi} \left\{ 2 \left[\frac{1 - \Sigma}{2\rho} \log \frac{\Delta^2 - (1 + \rho)^2}{\Delta^2 - (1 - \rho)^2} - 1 \right] \right. \\ & \times \left(\log \frac{2E_{\text{max}}}{\sqrt{M_K M_\pi}} + 1 \right) \\ & + \frac{\Delta}{2\rho} \log \frac{(\Delta + \rho)^2 - 1}{(\Delta - \rho)^2 - 1} + \frac{1}{2\rho} \log \frac{\Delta^2 - (1 + \rho)^2}{\Delta^2 - (1 - \rho)^2} \\ & + \frac{1 - \Sigma}{4\rho} \left[2 \text{Li} \left(\frac{2\rho}{\rho + \Delta - 1} \right) + 2 \text{Li} \left(\frac{2\rho}{\rho - \Delta + 1} \right) \right. \\ & - 2 \text{Li} \left(\frac{2\rho}{\rho - \Delta - 1} \right) - 2 \text{Li} \left(\frac{2\rho}{\rho + \Delta + 1} \right) \\ & \left. \left. - \log \frac{(\Delta + \rho)^2 - 1}{(\Delta - \rho)^2 - 1} \log \left(\frac{\Delta^2 - (1 + \rho)^2}{\Delta^2 - (1 - \rho)^2} \frac{M_K^2}{M_\pi^2} \right) \right] \right\}, \end{aligned} \quad (13)$$

where $\Sigma = (M_K^2 + M_\pi^2)/s$, $\Delta = (M_K^2 - M_\pi^2)/s$, and $\rho = \lambda^{1/2}/s$. We note that also $\omega_{K\pi}$ is ultraviolet finite and does not require a counterterm. The contribution of graphs with a virtual-photon coupling to the $K \rightarrow \pi \gamma^*$ vertex, see Fig. 3, is essential for this cancelation to work. This vertex, with full dependence on the form factor $F(s)$, can be constructed from gauge invariance requirements along the same lines discussed in Refs. [22, 23] (for the bremsstrahlung parts in $K_{\ell 3\gamma}$). We find therefore that *all* graphs contributing to radiative corrections in $d\Gamma/ds$ as shown in Figs. 1 and 3 depend on the full form factor $F(s)$ without constraints on its functional form, so $F(s)$ can be fully factorized, and the correction factors Ω are independent of it. [This of course ceases to be true once “internal” radiative corrections are included as e.g. pho-

ton exchange within a charged meson loop contribution to the form factor; see Ref. [21].]

We also show the correction factor $\Omega(K^+ \rightarrow \pi^+ \mu^+ \mu^-)$ (in the soft-photon approximation) in Fig. 2. The additional term is seen to increase it compared to the neutral kaon channel by a smooth function contributing about 1% to 1.5%.

3.2 $K \rightarrow \pi e^+ e^-$

Inserting the electron mass m_e into the correction factor in the soft approximation, Eq. (9), or the exact form in Appendix A, leads to two observations that may seem unsettling at first sight. First, the correction factor $\Omega_{e^+e^-}$ is large, up to 10% or so, despite the fact that the Coulomb pole that is the dominant effect in the muon channel is hardly visible, as its characteristic extension is now given by the scale of the electron mass and hence tiny. Second, there are much more severe deviations between the exact form and the soft-photon approximation, even though both lead to results larger than naïvely expected.

The explanation for this behavior can be found by expanding $\Omega_{e^+e^-}$ from Eq. (A.1) in the electron mass, neglecting terms of $\mathcal{O}(m)$, which leads to

$$\begin{aligned} \Omega_{e^+e^-} = & \frac{\alpha}{\pi} \left\{ \frac{1}{4} - 2 \left[\log \epsilon + \frac{(1 - \epsilon)(3 - \epsilon)}{4} \right] \log \delta \right. \\ & + \frac{1 - \epsilon}{2} \left[(3 - \epsilon) \log(1 - \epsilon) - \frac{11 - 3\epsilon}{2} \right] \\ & \left. - 2 \log \epsilon + \frac{\pi^2}{3} - 2 \text{Li}(\epsilon) \right\} + \mathcal{O}(m), \end{aligned} \quad (14)$$

with $\epsilon = 2E_{\text{max}}/\sqrt{s}$ and $\delta = m^2/s$. The result for the $\log \delta$ enhanced terms is in agreement with Ref. [24]. Numerically, one finds that this reproduces the exact form to an accuracy of 10^{-6} . Equation (14) contains terms that diverge logarithmically in the limit of the electron mass approaching zero, so-called Sudakov logarithms. This is not in contradiction with the Kinoshita–Lee–Nauenberg theorem [25, 26], which only states the absence of such mass singularities in *inclusive* transition probabilities. Indeed, it is easy to check that in the inclusive limit, corresponding to $\epsilon = 1$ in Eq. (14), all terms $\propto \log \delta$ vanish, and the whole correction factor reduces to $\Omega_{e^+e^-} = \alpha/4\pi + \mathcal{O}(m)$. We also understand why the soft-photon approximation is insufficient: it amounts to neglecting all terms of $\mathcal{O}(\epsilon)$ in Eq. (14), which changes the coefficient of the mass logarithm and fails to yield the required cancelation in the inclusive limit.

The origin of the electron mass singularities is well understood: they stem from photons radiated collinearly off the (nearly massless) electrons. The close-to-on-shell electron propagator in a bremsstrahlung diagram, with a photon of momentum l , is of the form

$$\frac{1}{2p-l} = \frac{1}{2 \left(\sqrt{m^2 + \mathbf{p}_-^2} - |\mathbf{p}_-| \cos \theta_{e-\gamma} \right) |l|}, \quad (15)$$

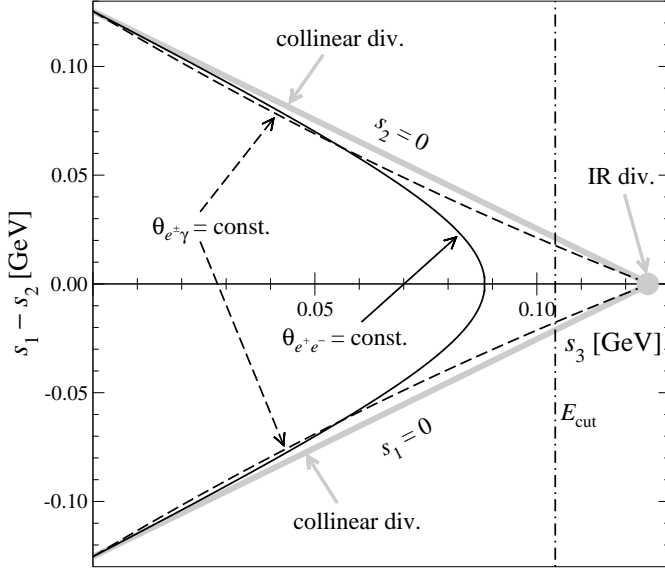


Fig. 4. Dalitz plot for $\gamma^* \rightarrow e^+e^-\gamma$ at maximal $s = (M_K - M_\pi)^2$. Shown are the positions of the collinear singularities for $s_1 = 0$ and $s_2 = 0$ (broad grey bands) as well as the infrared singularity at their intersection (thick grey dot). Drawn relative to those are various cut positions in $\theta_{e\pm\gamma}$ (dashed line), E_{\max} (vertical dash-dotted), and $\theta_{e^+e^-}$ (full black).

which in the limit $m \rightarrow 0$ diverges in forward direction, $\cos\theta_{e-\gamma} = 1$. To illuminate the structure of the various divergences, we show a sketch of the Dalitz plot for the decay $\gamma^*(p-k) \rightarrow e^+(p_+)e^-(p_-)\gamma(l)$ in Fig. 4, for a “mass” of the decaying virtual photon corresponding to the kinematic maximum $\sqrt{s_{\max}} = M_K - M_\pi$. We discuss this sub-decay in terms of three Mandelstam variables $s_{1/2} = (p_\mp + l)^2$, $s_3 = (p_+ + p_-)^2$, obeying $s_1 + s_2 + s_3 = s + 2m^2 \approx s$ in the massless limit, where the Dalitz plot degenerates into a triangle. Figure 4 shows the collinear singularities occurring along the lines $s_1 \approx 0$, $s_2 \approx 0$, as well as the infrared singularity at $l = 0$ at the intersection of those two lines. It is obvious that excluding all photons with an energy above E_{cut} leaves mass singularities in the resulting corrections, stemming precisely from hard collinear photons.

However, much as the inclusion of soft photons in a realistic measurement is an experimental requirement due to finite detector energy resolution, so is the inclusion of collinear photons due to finite angular resolution. We therefore have to cut not only on the photon energy, but also on the angles $\theta_{e\pm\gamma}$.¹ Figure 4 shows the position of such an angular cut in the $e^+e^-\gamma$ Dalitz plot: obviously, the hard collinear photons are now part of the correction factor. The result for $\Omega_{e^+e^-}$ with such an angular cut is

¹ This of course also holds true in principle for bremsstrahlung off heavy particles, such as the muon decay channel discussed in the previous section. However, without any strong collinear enhancement, the excision of photons at relative angles below, say, 20° from the full solid angle leads to a modification of the correction factor below the permille level—a negligible effect.

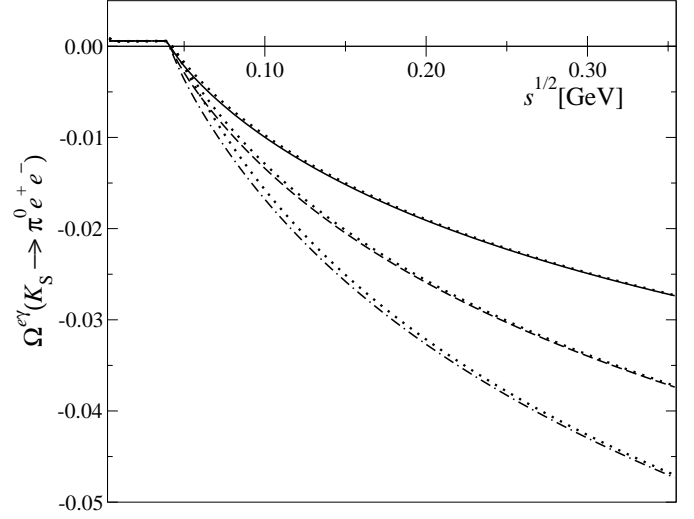


Fig. 5. Correction factor for $d\Gamma/ds(K_S \rightarrow \pi^0 e^+e^-)$ in the massless limit, with cuts on $\theta_{e\pm\gamma} = 20^\circ$ (full line), 10° (dashed), and 5° (dash-dotted), all with $E_{\text{cut}} = 20$ MeV. For comparison, the dotted lines nearby show the same curves for the physical electron mass.

given, in the massless limit ($m = 0$), as

$$\begin{aligned} \Omega_{e^+e^-}^{e\gamma} = & \frac{\alpha}{\pi} \left\{ \frac{1}{4} - 2 \left[\log \epsilon + \frac{(1-\epsilon)(3-\epsilon)}{4} \right] \log \frac{1-c_{e\gamma}}{1+c_{e\gamma}} \right. \\ & - \frac{1-\epsilon}{2} \left[(3-\epsilon) \log(1-\epsilon) - \frac{11-3\epsilon}{2} - \frac{8}{1-c_{e\gamma}} \right. \\ & \times \left(\frac{1+c_{e\gamma}}{(1-\epsilon)(1-c_{e\gamma})} \log \left(\epsilon + \frac{2(1-\epsilon)}{1+c_{e\gamma}} \right) - 1 \right) \\ & \left. \left. - \frac{\pi^2}{3} + 2 \text{Li}(\epsilon) \right] \right\}, \end{aligned} \quad (16)$$

with $c_{e\gamma} = \cos\theta_{e\pm\gamma}$. Equation (16) holds for realistic (small) angular cuts; for $\cos\theta_{e\pm\gamma} < -\epsilon/(2-\epsilon)$, i.e. basically with all photons radiated in the forward direction relative to electron and positron cut out, the angular cut alone becomes more restrictive than the photon-energy cut, and the above formula has to be continued with the replacement $\epsilon \rightarrow -2c_{e\gamma}/(1-c_{e\gamma})$. The result then translates smoothly into the fully inclusive one for $c_{e\gamma} \rightarrow -1$. On the other hand, for small angles or $c_{e\gamma} \approx 1$, Eq. (16) shows how the mass singularity in Eq. (14) is translated into a kinematical or phase space singularity.

$\Omega_{e^+e^-}^{e\gamma}$ is displayed graphically for three different angular cuts in Fig. 5, all with $E_{\text{cut}} = 20$ MeV. For comparison, Fig. 5 also shows, in addition to the massless result Eq. (16), the exact result with finite electron mass, obtained numerically: the differences are tiny. Obviously the correction factor is largest with the tightest cut on the angle, however for realistic angles, it is small over the whole dilepton distribution range, on the level of 2% to 4%.

There is another possibility how to apply phase space cuts such as to cover all the singular regions in the bremsstrahlung that is maybe slightly less obvious, namely to cut on the positron–electron angle $\theta_{e^+e^-}$. All singularities,

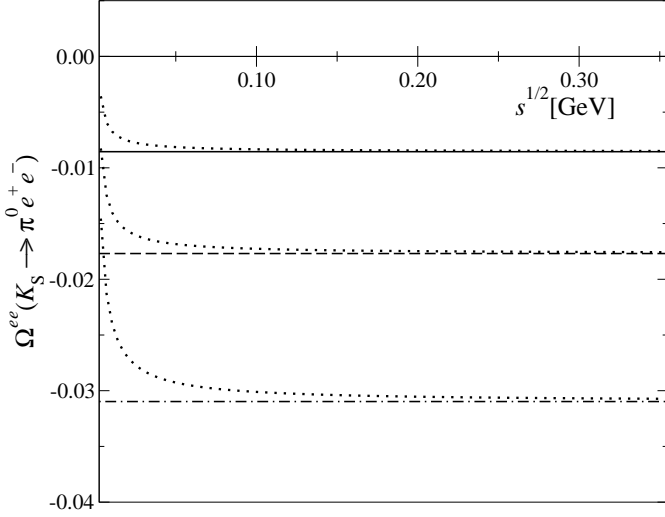


Fig. 6. Correction factor for $d\Gamma/ds(K_S \rightarrow \pi^0 e^+ e^-)$ in the massless limit, with cuts on $\theta_{e^+e^-} = 160^\circ$ (full line), 170° (dashed), and 175° (dash-dotted). For comparison, the dotted lines nearby show the same curves for the physical electron mass.

both the infrared divergence and the collinear ones, occur for electron and positron back-to-back, i.e. $\cos\theta_{e^+e^-} \approx -1$. A line of constant $\theta_{e^+e^-}$ is also shown in Fig. 4. The result for $\Omega_{e^+e^-}$ with such an e^+e^- collinear cut applied, again in the massless limit, is given by

$$\Omega_{e^+e^-}^{ee} = \frac{\alpha}{\pi} \left\{ \frac{1}{4} + \text{Li} \left(\frac{c_{ee} - 1}{c_{ee} + 1} \right) - \frac{9 - 5c_{ee}}{4(1 - c_{ee})} - 2 \frac{2 - c_{ee}}{(1 - c_{ee})^2} \log \frac{1 + c_{ee}}{2} \right\}, \quad (17)$$

with $c_{ee} = \cos\theta_{e^+e^-}$. Equation (17) again is in accordance with Ref. [24]. With no cut on any dimensionful quantity applied (and $m = 0$), $\Omega_{e^+e^-}^{ee}$ is bound to be a constant. Comparison to results at finite electron mass obtained numerically for three different cut angles, see Fig. 6, show some deviations for very small s . Again, with realistic angular cuts, the resulting correction factors are small on the few-percent level.

Finally, after this extensive discussion of $\Omega_{e^+e^-}$ with various cuts and approximations, which directly yields the correction factor $\Omega(K_S \rightarrow \pi^0 e^+ e^-)$, we have to remark on the phenomenologically most relevant case, $K^+ \rightarrow \pi^+ e^+ e^-$. As for $K^+ \rightarrow \pi^+ \mu^+ \mu^-$, we have to add the corrections on the hadronic side $\Omega_{K\pi} = \omega_{K\pi}$ to obtain the full result for $d\Gamma/ds$. It is fully justified to use the soft-photon approximation Eq. (13) for this part, as it does not involve the lepton mass at all and hence shows no enhancement for $m \rightarrow 0$. An analytic implementation of angular cuts in the $e^+e^- \gamma$ system on $\Omega_{K\pi}$ is not feasible, however it is also not necessary, as there are no collinear enhancements, and the angular cuts only remove a very small part of the solid angle. Estimating the effect of a cut on the lepton-photon angle of 20° leads to a modification of the correction factor of a few times 10^{-4} and can hence safely be disregarded.

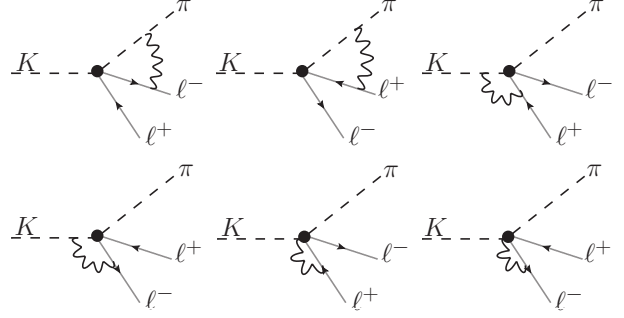


Fig. 7. Feynman graphs contributing to the $\ell^+ \ell^-$ asymmetry in $K^+ \rightarrow \pi^+ \ell^+ \ell^-$ through virtual-photon corrections. The real-photon contributions via interference of lepton and meson bremsstrahlung, see Figs. 1 and 3 respectively, are not displayed again.

4 $\ell^+ \ell^-$ asymmetry

There is a set of radiative corrections in $K^+ \rightarrow \pi^+ \ell^+ \ell^-$ not considered so far, namely virtual-photon corrections linking the hadronic and the leptonic currents, see Fig. 7, plus the interference terms of bremsstrahlung from leptons with bremsstrahlung from mesons. All these contributions are odd under exchange of ℓ^+ and ℓ^- and hence cancel in $d\Gamma/ds$, see Eq. (7). However, they induce an $\ell^+ \ell^-$ (or $t-u$) asymmetry, which we define in a normalized way as

$$A_\nu(s) = \left(\frac{d\Gamma}{ds} \right)^{-1} \int d\nu \text{sgn}(\nu) \frac{d^2\Gamma}{ds d\nu}, \quad (18)$$

where $\text{sgn}(x)$ is the sign function. With this definition, the asymmetry is independent of overall coupling constants, and we expect it to be on the typical level of radiative correction effects, i.e. a few percent at most. Referring back to Eq. (6), we can re-express A_ν in a very simple form in terms of the correction factors $\hat{\omega}$ and $\tilde{\omega}$ as

$$A_\nu(s) = \frac{1}{\lambda^{3/2} \sigma (1 - \sigma^2/3)} \int_0^{\sigma \lambda^{1/2}} d\nu [(\lambda - \nu^2) \hat{\omega} + m^2 \nu \tilde{\omega}]. \quad (19)$$

The explicit results for $\hat{\omega}$ and $\tilde{\omega}$ are significantly more complicated and lengthy than those shown so far and are therefore relegated to Appendix B. Several features of these corrections however need to be discussed in some detail. First, in contrast to what we found for the corrections to the dilepton spectra, $\hat{\omega}$ and $\tilde{\omega}$ are not automatically ultraviolet finite. Naturally, nothing is known about the finite coefficients of the required counterterms, whose effects we therefore have to estimate by different means. We do this by employing the corresponding ultraviolet scale dependence of the loop contributions: choosing the mass of the ρ as a natural central scale, we vary it by a factor of $e = 2.71 \dots$, i.e. between $0.37 M_\rho$ and $2.71 M_\rho$. We believe this to be a reasonable uncertainty estimate.

Second, also in contrast to the correction factors for the dilepton distributions, the dependence on the form factor $F(s)$ does not factorize any longer in the loop contributions of Fig. 7. In fact, a hadronic loop in $F(s)$ would

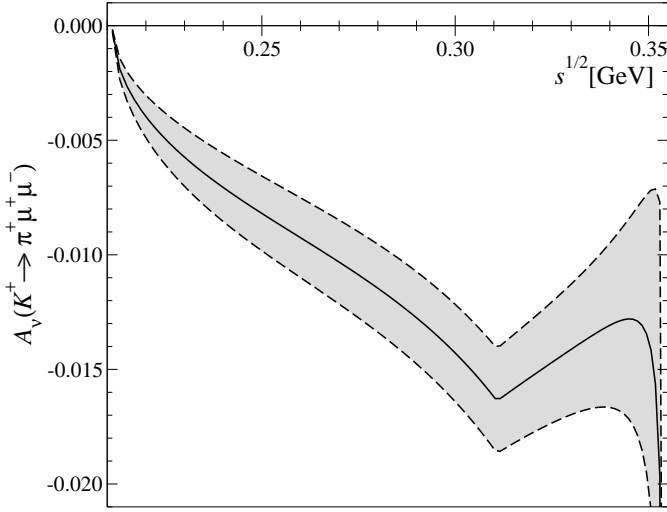


Fig. 8. The asymmetry $A_\nu(K^+ \rightarrow \pi^+ \mu^+ \mu^-)$ according to Eq. (18). The width of the grey band mirrors the uncertainty due to an unknown counterterm, mimicked by varying the ultraviolet scale between $0.37M_\rho$ and $2.71M_\rho$.

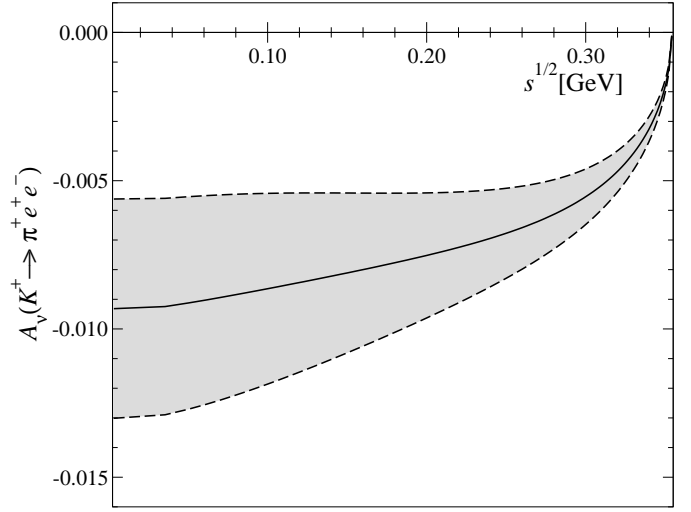


Fig. 9. The asymmetry $A_\nu(K^+ \rightarrow \pi^+ e^+ e^-)$ according to Eq. (18). The width of the grey band mirrors the uncertainty due to an unknown counterterm, mimicked by varying the ultraviolet scale between $0.37M_\rho$ and $2.71M_\rho$.

immediately lead to non-trivial (i.e. non-factorizing) two-loop graphs for the photon corrections. As already indicated in the introduction, we approximate such effects by assuming a linear form factor, with the slope as measured in Ref. [8], $F'(0)/F(0) = (2.32 \pm 0.18)M_K^{-2}$. The correction factors $\hat{\omega}$, $\tilde{\omega}$ then contain terms that depend on $F'(s)/F(s)$.

There is another subtlety in the calculation of the graphs in Fig. 7. We have always drawn Feynman diagrams with point-like $K\pi\ell^+\ell^-$ vertices, owing to the fact that the first term in the form factor definition Eq. (1) contains a factor of s , canceling the photon propagator. In contrast to all graphs in Figs. 1 and 3, the second term in the form factor $\propto (k^2 - p^2)(k - p)^\mu$, which does not contain such a factor of s , does not vanish any more diagram by diagram for loop contributions with photons linking mesons to fermions. The cancellation of apparent two-photon-cut contributions in the full result is hence a useful check on the calculation.

Finally, we only include bremsstrahlung in the soft-photon approximation (thereby in particular eschewing the non-trivial question of how to properly *define* the asymmetry, once the real-photon momentum is not neglected in the kinematic relations), also for the electron-positron final state. We deem this justified for two reasons: first, we find that the electron mass or collinear singularities actually cancel in the asymmetry Eq. (19), hence there is a smooth limit of the electron mass approaching zero, no unnatural enhancement occurs, and there is no need to further cut on the angles in the phase space integral. Second, the remaining uncertainty inherent in the soft approximation we consider well-covered by the sizeable (as we shall see below) error due to the ultraviolet scale dependence discussed above.

The resulting asymmetries $A_\nu(s)$ are displayed in Fig. 8 for $K^+ \rightarrow \pi^+ \mu^+ \mu^-$ and in Fig. 9 for $K^+ \rightarrow$

$\pi^+ e^+ e^-$. Both are shown for a photon-energy cut of $E_{\text{cut}} = 20$ MeV; the variation of the cutoff by 10 MeV leads to changes in the asymmetries significantly below the ranges displayed by the grey bands, which represent the estimated uncertainties due to the ultraviolet counterterm. Similarly, the error due to the experimental uncertainty in the slope of the form factor quoted above is totally negligible in comparison. The main features of the results shown in Figs. 8 and 9 can be readily understood:

1. The sign of the asymmetry is negative: positive ν corresponds to large t and small u , or a small invariant mass of π^+ and ℓ^+ , for which the repulsion of the two positively charged particles in the final state dominates; vice versa, for negative ν or small t , the attraction between π^+ and ℓ^- leads to an enhancement.
2. The asymmetry for the muon channel vanishes for small $s \rightarrow 4m^2$: due to the integration limit $\nu_{\text{max}} = \sigma\lambda^{1/2}$, the fact that $\hat{\omega}$ is odd in ν , plus the explicit factor of ν in front of $\tilde{\omega}$, it is obvious that the numerator in Eq. (19) has one more power of σ than the denominator, hence $A_\nu(s)$ vanishes square-root-like at the lower end of the spectrum. This effect is invisible in the electron asymmetry due to the smallness of the electron mass, for which effectively $\sigma \approx 1$.
3. A similar argument explains the behavior at the upper end of the spectrum, for large $s \rightarrow (M_K - M_\pi)^2$: were it only for the correction factor $\hat{\omega}$, the numerator would be suppressed compared to the denominator by a factor of $\lambda^{1/2}$, and the asymmetry would approach zero; however the term $\propto \tilde{\omega}$, when integrated over ν , is *enhanced* by a factor of $\lambda^{1/2}$, hence the divergence seen in the muon asymmetry. On the other hand, $\tilde{\omega}$ comes with a prefactor of m^2 , such that this term is negligible in the electron channel, where we therefore indeed see the asymmetry going to zero at the upper limit of phase space.

4. Finally, there appears to be a cusp-like structure in the muon asymmetry, Fig. 8. This can be traced back to the ν integration hitting the Coulomb poles in the t and u channels, which happens for $s^* = m(M_K^2 - M_\pi^2)/(M_\pi + m)$. The Coulomb pole is an integrable singularity of the form $(t - t_{\text{thr}})^{-1/2}$ (at this order in α), which is touched tangentially by the integration (phase space) limit, leading to a non-regular behavior of the type

$$\int_{t_{\min}(s)} \frac{dt}{\sqrt{t - t_{\text{thr}}}} \simeq \int_{k(s-s^*)^2} \frac{dt}{\sqrt{t}} \propto \sqrt{(s - s^*)^2}, \quad (20)$$

hence like an absolute-value function. Again, as s^* scales with m , this non-regular behavior practically coincides with the threshold in the electron channel and is therefore invisible in Fig. 9.

The overall size of the two asymmetries is indeed typical for an electromagnetic effect on hadronic observables, it lies in the range of 1%–2%. The asymmetry for the electron channel shows no enhancement, and is virtually identical to the one in the zero mass limit.

5 $P \rightarrow V \ell^+ \ell^-$ and $V \rightarrow P \ell^+ \ell^-$ decays

It is obvious that any decay $P \rightarrow P' \ell^+ \ell^-$ dominated by one-photon exchange, where P, P' denote pseudoscalar mesons, will have the same universal electromagnetic correction effects as discussed in the previous sections. They only depend on the structure of the hadronic current, Eq. (1), which in turn is dictated by parity and gauge invariance, so the central results can be readily adapted for e.g. charm or bottom decays, with the appropriate mass replacements.

The transfer of our calculations to decays of the type $P \rightarrow V \ell^+ \ell^-$ or $V \rightarrow P \ell^+ \ell^-$, for pseudoscalar P and vector V mesons, may be less obvious. Physical processes of these types, as already mentioned in the introduction, include the π^0 and η Dalitz decays $\pi^0 \rightarrow \gamma e^+ e^-$ (see e.g. Ref. [27] for theoretical work on this decay), $\eta \rightarrow \gamma \ell^+ \ell^-$ [28], or the vector meson conversion decays such as $\omega \rightarrow \pi^0 \ell^+ \ell^-$ or $\phi \rightarrow \eta \ell^+ \ell^-$ [29]. Reference [27] gives a detailed account on radiative corrections in $\pi^0 \rightarrow \gamma e^+ e^-$ far beyond the universal effects considered here, however relying mainly on the soft approximation for the real-photon radiation and without an analysis of collinear singularities and angular phase space cuts.

We generically denote decays of these types by $A(k) \rightarrow B(p) \ell^+(p_+) \ell^-(p_-)$, with $M_{A/B}$ the masses of A and B ($M_B = 0$ for the π^0 or η Dalitz decays). What is common to these channels is that they involve anomalous decay vertices of odd intrinsic parity, so the hadronic vector current is written in terms of the Levi-Civita tensor,

$$\langle B(p) | J_{\text{em}}^\mu(0) | A(k) \rangle \propto \epsilon^{\mu\nu\alpha\beta} \epsilon_\nu^* k_\alpha p_\beta F(s), \quad (21)$$

where the form factor F is again a function of $s = (k - p)^2$, and we have spelled out the case of the $P \rightarrow V$ decay, with

ϵ_ν^* the polarization vector of the outgoing B . Equation (21) can be transformed into the $V \rightarrow P$ case by the simple replacement $\epsilon_\nu^* \rightarrow \epsilon_\nu$, ϵ_ν then being the polarization vector of the incoming A .

It is conventional to normalize the rates by the real-photon width $\Gamma_0 \doteq \Gamma(A \rightarrow B \gamma)$ (which, in contrast to $K \rightarrow \pi \gamma$, is not required to vanish by gauge invariance). Including radiative correction factors, we can write the Dalitz plot distribution as

$$\frac{d\Gamma}{\Gamma_0} = \frac{n \alpha |\bar{F}(s)|^2}{8\pi s (M_A^2 - M_B^2)^3} \left[((2 - \sigma^2) \lambda + \nu^2) (1 + \omega) + (\sigma^2 \lambda - \nu^2) \bar{\omega} \right] ds d\nu, \quad (22)$$

where $\lambda \doteq \lambda(M_A^2, s, M_B^2)$, $\nu = t - u$ defined as before, $\bar{F}(s) = F(s)/F(0)$ is the normalized form factor, and $n = 1$ for vector meson conversion and $n = 2$ for pseudoscalar Dalitz decays. ω and $\bar{\omega}$ are the *same* corrections factors of $\mathcal{O}(\alpha)$ as discussed in various forms and approximations in Sect. 3. We only consider processes with uncharged bosons (as in all the sample processes mentioned above), so we do not include the correction terms odd in $t - u$. The resulting dilepton invariant mass spectrum is

$$\frac{d\Gamma}{ds \Gamma_0} = \frac{n \alpha |F(s)|^2}{2\pi s (M_A^2 - M_B^2)^3} \lambda^{3/2} \sigma \left(1 - \frac{\sigma^2}{3}\right) (1 + \Omega), \quad (23)$$

where Ω is again given in terms of ω and $\bar{\omega}$ by the same relation Eq. (7) as in $K \rightarrow \pi \ell^+ \ell^-$. So while the Dalitz plot distribution Eq. (22) is entirely different from that of Eq. (3), owing to the different spin of one of the bosons involved, the dilepton mass spectrum and its radiative correction factor look, apart from the different form factors involved, the same. We emphasize that this also holds for the bremsstrahlung contributions beyond the soft-photon approximation, for which this is far from obvious in the course of the calculation; see Appendix C for details.

6 Summary and conclusion

We have calculated the universal radiative corrections for meson decay processes with a lepton–antilepton pair in the final state, in particular the flavor-changing neutral current process $K \rightarrow \pi \ell^+ \ell^-$, with the following main results.

1. For the most interesting observable, the differential spectrum with respect to the invariant mass of the dilepton pair, radiative corrections at $\mathcal{O}(\alpha)$ are given as a simple sum of corrections to the hadronic and the leptonic current, both of which are ultraviolet finite without requiring a counterterm.
2. For the muon final state, the soft-photon approximation with a cut on the additional photon energy in the bremsstrahlung contribution is very accurate and leads to an enhancement on the 1%–2% level, apart from the Coulomb pole close to threshold.

3. The (unphysical) excision of hard collinear bremsstrahlung photons leads to the survival of logarithmic mass singularities in the electron channels. This requires the introduction of additional angular cuts in the leptonic radiative corrections, either between bremsstrahlung photon and electron/positron, or on the electron-positron angle. We provide closed analytic results for the cut dependence of these correction factors in the limit of the electron mass going to zero, which is shown to be a very good approximation.
4. Radiative corrections in the charged decays $K^+ \rightarrow \pi^+ \ell^+ \ell^-$ that link the hadronic and the leptonic current are odd under exchange of ℓ^+ and ℓ^- . They cancel in the dilepton spectrum, but induce an $\ell^+ \ell^-$ asymmetry on the level of 1%–2%. This asymmetry is free of small mass singularities and not enhanced in the electron case, but requires ultraviolet renormalization via a counterterm that induces a sizeable uncertainty.
5. Finally, we have shown that the universal correction factors for the dilepton spectra can be directly used also for other decays such as π^0 or η Dalitz decays or vector meson conversion decays like $\omega \rightarrow \pi^0 \ell^+ \ell^-$, despite a different form of the hadronic vector current involved.

These results ought to provide a useful and necessary ingredient in future precision measurements of the decay processes concerned.

Acknowledgements We would like to thank Gino Isidori for suggesting to undertake this study, and for extensive advice and helpful discussions along the way. Furthermore, we thank Guido Bell for useful e-mail communications. Partial financial support by the Helmholtz Association through funds provided to the virtual institute “Spin and strong QCD” (VH-VI-231), by the Integrating Activity project “Study of Strongly Interacting Matter” (acronym HadronPhysics2, grant agreement No. 227431) under the Seventh Framework Programme of the EU, and by DFG (SFB/TR 16, “Subnuclear Structure of Matter”) is gratefully acknowledged.

A Correction factor $\Omega(K_S \rightarrow \pi^0 \ell^+ \ell^-)$

In this appendix we show the analytic form of the correction factor $\Omega_{\ell^+ \ell^-}$ beyond the soft-photon approximation discussed in Sect. 3.1, i.e. with the exact E_{\max} and full mass dependence, but without any additional angular cuts. We find

$$\begin{aligned} \Omega_{\ell^+ \ell^-} = & \Omega_{\ell^+ \ell^-}^{\text{soft}} + \frac{\alpha}{\pi} \left\{ \frac{1+\sigma^2}{\sigma} \left[2 \text{Li} \left(\frac{1-\sigma}{1+\sigma} \right) - \text{Li} \left(\frac{1-\sigma_\epsilon}{1+\sigma} \right) \right. \right. \\ & - \text{Li} \left(\frac{1-\sigma}{1+\sigma_\epsilon} \right) + \text{Li} \left(\frac{1+\sigma}{2} \right) - \text{Li} \left(\frac{1+\sigma_\epsilon}{2} \right) \\ & - \text{Li} \left(\frac{1-\sigma}{2} \right) + \text{Li} \left(\frac{1-\sigma_\epsilon}{2} \right) + \text{Li} \left(\frac{1+\sigma_\epsilon}{1+\sigma} \right) - \frac{\pi^2}{3} \\ & \left. \left. + \text{Li} \left(\frac{1-\sigma}{1-\sigma_\epsilon} \right) - \log \left(\frac{1+\sigma}{1-\sigma} \frac{1-\sigma_\epsilon}{1+\sigma_\epsilon} \right) \log \frac{2\epsilon}{1+\sigma} \right] \right. \\ & \left. + 4 \log \frac{\sigma+\sigma_\epsilon}{2\sigma} - \frac{\epsilon}{\sigma} \left(2 - \frac{\epsilon}{3-\sigma^2} \right) \log \frac{1+\sigma_\epsilon}{1-\sigma_\epsilon} \right\} \end{aligned}$$

$$\begin{aligned} & + 2 \log(1-\epsilon) + \frac{9-2\sigma^2+\sigma^4}{8\sigma(3-\sigma^2)} \log \left(\frac{1+\sigma}{1-\sigma} \frac{1-\sigma_\epsilon}{1+\sigma_\epsilon} \right) \\ & + \frac{\sigma-\sigma_\epsilon}{\sigma(1-\sigma_\epsilon^2)} \left[(1+\sigma\sigma_\epsilon) \left(4 + \frac{3(1-\epsilon)}{2(3-\sigma^2)} \right) \right. \\ & \left. - \frac{(9+\sigma^2)\sigma\sigma_\epsilon}{4(3-\sigma^2)} - \frac{5}{4} \right] \Bigg\} , \end{aligned} \quad (\text{A.1})$$

with $\sigma_\epsilon = \sqrt{(\sigma^2 - \epsilon)/(1 - \epsilon)}$ and $\epsilon = 2E_{\max}/\sqrt{s}$. It is easy to see from Eq. (A.1) that $\Omega_{\ell^+ \ell^-} - \Omega_{\ell^+ \ell^-}^{\text{soft}} = \mathcal{O}(E_{\max})$. The numerical evaluation and comparison of this result to the soft approximation for the muon final state is shown in Fig. 2. Equation (A.1) also allows to easily derive e.g. the fully inclusive correction factor, i.e. without phase space cuts on the real-photon emission, for finite mass m ; this corresponds to the limit $\epsilon = \sigma^2$.

B Contributions to the $\ell^+ \ell^-$ asymmetry

The radiative correction factors $\hat{\omega}$ and $\tilde{\omega}$, defined in Eq. (6) and discussed numerically in Sect. 4, are given analytically by the expressions

$$\begin{aligned} \hat{\omega} = & 8\pi\alpha \left\{ H_\pi^{(1)}(u) - H_\pi^{(1)}(t) + H_K^{(1)}(u) - H_K^{(1)}(t) \right. \\ & \left. + \frac{F'(s)}{F(s)} \left[V_{\pi K}^{(1)}(u) - V_{\pi K}^{(1)}(t) + V_{K\pi}^{(1)}(u) - V_{K\pi}^{(1)}(t) \right] \right\} \\ & + \frac{\alpha}{\pi} \int_{-1}^1 d\xi \left[F_\pi(t, \xi) - F_\pi(u, \xi) + F_K(u, \xi) - F_K(t, \xi) \right] , \\ \tilde{\omega} = & 64\pi\alpha \left\{ H_\pi^{(2)}(t) + H_\pi^{(2)}(u) + H_K^{(2)}(t) + H_K^{(2)}(u) + \frac{3\Delta_\ell}{m^2} \right. \\ & - \frac{1}{16\pi^2} + \frac{F'(s)}{F(s)} \left[V_{\pi K}^{(2)}(t) + V_{\pi K}^{(2)}(u) + V_{K\pi}^{(2)}(t) + V_{K\pi}^{(2)}(u) \right. \\ & \left. \left. + 4\Delta_\ell + \frac{m^2}{8\pi^2} - s \left(\frac{5\Delta_\ell}{3m^2} + \frac{1}{18\pi^2} \right) \right] \right\} . \end{aligned} \quad (\text{B.1})$$

As discussed in the main text, the $K \rightarrow \pi \gamma^*$ form factor is approximated by a linear form, inducing the terms $\propto F'(s)/F(s)$ in Eq. (B.1). We have defined the following combinations of loop functions:

$$\begin{aligned} H_a^{(1)}(x) = & (x - m^2 - M_a^2) [2G_a(x) - G_a^+(x) + 3G_a^-(x)] \\ & - 2(M_a^2 + m^2)G_a^+(x) - 2(M_a^2 - m^2)G_a^-(x) - \bar{J}_a(x) , \\ H_a^{(2)}(x) = & (x - m^2) [G_a^+(x) - G_a^-(x)] , \\ V_{ab}^{(1)}(x) = & (M_b^2 - M_a^2) (m^2 + M_a^2 + x) G_a^{(1)}(x) \\ & + \frac{1}{4} (M_b^2 - M_a^2 - 2s) (7m^2 + 3M_a^2 - 5x) G_a^-(x) \\ & + \frac{1}{2} \left[s(x + m^2 + M_a^2) \right. \\ & \left. - (M_b^2 - M_a^2) (3(x - m^2) - M_a^2) \right] G_a^+(x) \\ & + \frac{1}{2} \left[\frac{(M_b^2 - M_a^2 - 2m^2)(M_a^2 - m^2)}{x} + s + 2x \right] \end{aligned}$$

$$\begin{aligned}
& + M_b^2 - 3M_a^2 - 4m^2 \Big] \bar{J}_a(x) - x \frac{\Delta_a - \Delta_\ell}{M_a^2 - m^2} , \\
V_{ab}^{(2)}(x) = & (x - m^2) \left[(M_a^2 - M_b^2) G_a^{(1)}(x) \right. \\
& + \frac{1}{4} (M_a^2 - M_b^2 + 2s) G_a^-(x) - \frac{s}{2} G_a^+(x) \\
& \left. + \frac{x + M_a^2 - m^2}{2x} \bar{J}_a(x) - \frac{\Delta_a - \Delta_\ell}{2(M_a^2 - m^2)} \right] . \quad (\text{B.2})
\end{aligned}$$

Here, the tadpole loop function contains the ultraviolet divergence in dimensional regularization,

$$\begin{aligned}
\Delta_a = & 2M_a^2 \left[L + \frac{1}{16\pi^2} \log \frac{M_a}{\mu} \right] , \\
L = & \frac{\mu^{d-4}}{16\pi^2} \left[\frac{1}{d-4} + \frac{1}{2} (\gamma_E - 1 - \log 4\pi) \right] , \quad (\text{B.3})
\end{aligned}$$

μ is the running (ultraviolet) scale, and we have made implicit use of the notation $M_\ell \doteq m$ for the lepton tadpole function Δ_ℓ above. Of the loop functions $\bar{J}_a(s)$ and $G_a(s)$, we only need the real parts in the two kinematical regimes $0 < s \leq (M_a - m)^2$ or $s \geq (M_a + m)^2$, where they are given by

$$\begin{aligned}
\text{Re} \bar{J}_a(s) = & \frac{1}{16\pi^2} \left\{ 1 + \left[\frac{M_a^2 - m^2}{s} - \frac{M_a^2 + m^2}{M_a^2 - m^2} \right] \log \frac{m}{M_a} \right. \\
& \left. - \frac{\sqrt{\lambda}}{2s} \log \frac{s - M_a^2 - m^2 + \sqrt{\lambda}}{s - M_a^2 - m^2 - \sqrt{\lambda}} \right\} , \quad (\text{B.4})
\end{aligned}$$

with the Källén function $\lambda = \lambda(s, M_a^2, m^2)$ used here and below, and by

$$\begin{aligned}
\text{Re} G_a(s) = & \frac{1}{32\pi^2 \lambda^{1/2}} \left\{ 2 \left(\log \frac{1 - z_2}{1 - z_1} + \log \frac{z_1}{z_2} \right) \log \frac{2E_{\max}}{\sqrt{s}} \right. \\
& + \text{Li} \left(\frac{z_2 - z_1}{z_2} \right) - \text{Li} \left(\frac{z_1 - z_2}{z_1} \right) + \text{Li} \left(\frac{z_2 - z_1}{1 - z_1} \right) \\
& - \text{Li} \left(\frac{z_1 - z_2}{1 - z_2} \right) + \log^2 |1 - z_1| - \log^2 |1 - z_2| \\
& \left. + \log^2 |z_2| - \log^2 |z_1| - 2\pi^2 \theta(s - (M_a + m)^2) \right\} , \quad (\text{B.5})
\end{aligned}$$

respectively, where $\theta(x)$ is the Heaviside function, and

$$z_{1/2} = \frac{1}{2s} (s + M_a^2 - m^2 \mp \sqrt{\lambda}) . \quad (\text{B.6})$$

Note that we already have absorbed the infrared-divergent part of the bremsstrahlung in $G_a(s)$ in order to obtain a finite, regulator-independent function. The remaining loop functions used above are given by

$$\begin{aligned}
G_a^+(s) = & \frac{1}{\lambda} \left[(m^2 - M_a^2) \left(\bar{J}_a(s) - \frac{1}{16\pi^2} \right) \right. \\
& \left. + \frac{s - M_a^2 - m^2}{16\pi^2} \log \frac{M_a}{m} \right] , \\
G_a^-(s) = & \frac{1}{\lambda} \left[s \left(\bar{J}_a(s) - \frac{1}{16\pi^2} \right) \right.
\end{aligned}$$

$$\left. - \frac{s(M_a^2 + m^2) - (M_a^2 - m^2)^2}{16\pi^2(M_a^2 - m^2)} \log \frac{M_a}{m} \right] ,$$

$$\begin{aligned}
G_a^{(1)}(s) = & \frac{1}{4s} \left\{ (M_a^2 - m^2) G_a^+(s) - \bar{J}_a(s) \right. \\
& \left. + \frac{1}{16\pi^2} \left(\frac{M_a^2 + m^2}{M_a^2 - m^2} \log \frac{M_a}{m} - 1 \right) \right\} . \quad (\text{B.7})
\end{aligned}$$

Finally, the (finite) bremsstrahlung contribution given (in the soft-photon approximation) in terms of the one-parameter integral over ξ in Eq. (B.1) is specified by

$$\begin{aligned}
F_a(x, \xi) = & - \frac{x - M_a^2 - m^2}{p_a^2} \frac{d_a}{n_a} \log \frac{d_a + n_a}{d_a - n_a} , \\
p_{\pi/K}^2 = & (1 + \xi)^2 M_{\pi/K}^2 + (1 - \xi)^2 m^2 \\
& \pm (1 - \xi^2) (x - M_{\pi/K}^2 - m^2) , \\
d_{\pi/K} = & (1 + \xi) (M_K^2 - M_\pi^2 \mp s) + (1 - \xi) s , \\
n_{\pi/K} = & \sqrt{d_{\pi/K}^2 - 4s p_{\pi/K}^2} . \quad (\text{B.8})
\end{aligned}$$

As in the main text, these finite bremsstrahlung contributions are understood to be calculated for the photon-energy cutoff applied in the $\ell^+ \ell^- \gamma$ rest frame, or $\mathbf{k} - \mathbf{p} = 0$.

C Details on bremsstrahlung

In this appendix, we show some details on the calculation of bremsstrahlung contributions to $\Omega_{\ell^+ \ell^-}$ beyond the soft-photon approximation. We concentrate on the results for the correction factor to $d\Gamma/ds$. To describe the decay $K(k) \rightarrow \pi(p) \ell^+(p_+) \ell^-(p_-) \gamma(l)$, we make use of the extended set of variables

$$\begin{aligned}
s = & (k - p)^2 , \quad s_1 = (p_- + l)^2 , \quad s_2 = (p_+ + l)^2 , \\
s_3 = & (p_+ + p_-)^2 , \quad t_1 = (p + p_+)^2 , \quad t_2 = (k - p_-)^2 , \\
u_1 = & (k - p_+)^2 , \quad u_2 = (p + p_-)^2 , \quad (\text{C.1})
\end{aligned}$$

which are subject to the constraints

$$\begin{aligned}
s_1 + s_2 + s_3 = & s + 2m^2 , \\
s + t_i + u_i = & M_K^2 + M_\pi^2 + m^2 + s_i , \quad i = 1, 2 . \quad (\text{C.2})
\end{aligned}$$

We also use the combinations of variables

$$\nu_i = t_i - u_i , \quad i = 1, 2 , \quad \Sigma = \nu_1 + \nu_2 , \quad \Delta = \nu_1 - \nu_2 , \quad (\text{C.3})$$

and, as in the main text, $\lambda \doteq \lambda(M_K^2, s, M_\pi^2)$. The contribution resulting from the bremsstrahlung diagrams in Fig. 1 can be formulated as

$$\begin{aligned}
\Omega_{\ell^+ \ell^-}^{\text{brems}} = & \frac{3\alpha}{8\pi \lambda \sigma (3 - \sigma^2) s} \int \frac{d\Omega}{4\pi} ds_1 ds_2 \left\{ \frac{N_1}{(s_1 - m^2)^2} \right. \\
& \left. + \frac{N_2}{(s_2 - m^2)^2} + \frac{N_3}{(s_1 - m^2)(s_2 - m^2)} \right\} . \quad (\text{C.4})
\end{aligned}$$

Here, s_1 and s_2 are the chosen invariant variables for the integration of the Dalitz plot in the $\ell^+ \ell^- \gamma$ system (in the

rest frame of which the calculation is performed), and $d\Omega$ is the solid angle integral of this system relative to the vector $\mathbf{k} = \mathbf{p}$. The numerators N_i in Eq. (C.4), $i = 1, 2, 3$, are obtained by performing the spin and polarization sums,

$$\begin{aligned} N_1 &= -4 \left\{ 2m^2(\lambda - \nu_1^2) + (s_1 - m^2) (M_K^2 - M_\pi^2 + \nu_1) \Delta \right. \\ &\quad \left. + (s_1 - m^2) (s_2 - m^2) [2(M_K^2 + M_\pi^2) - s] \right\}, \\ N_2 &= -4 \left\{ 2m^2(\lambda - \nu_2^2) + (s_2 - m^2) (M_K^2 - M_\pi^2 - \nu_2) \Delta \right. \\ &\quad \left. + (s_1 - m^2) (s_2 - m^2) [2(M_K^2 + M_\pi^2) - s] \right\}, \\ N_3 &= 4 \left\{ 2(s_3 - 2m^2)(\lambda - \nu_1 \nu_2) - s_3 \Delta^2 + \frac{s_3 - s}{2} \Sigma^2 \right. \\ &\quad \left. - (M_K^2 - M_\pi^2 + \frac{\Delta}{2})(s_1 - s_2) \Sigma \right\}. \end{aligned} \quad (\text{C.5})$$

Note that the non-trivial kinematic prefactors in Eq. (C.4) only stem from the normalization to the non-radiative decay spectrum; once this is reversed, Eqs. (C.4) and (C.5) contain the complete information to reconstruct the full kinematic dependence of the decay distribution of the bremsstrahlung process.

The variables with non-trivial angular dependence are $\nu_{1/2}$ or Σ , Δ , respectively, which upon integration over the solid angle yield

$$\begin{aligned} \int \frac{d\Omega}{4\pi} \left\{ \Delta, \Sigma, \Delta^2, \Sigma^2, \Delta\Sigma \right\} &= \left\{ (M_K^2 - M_\pi^2) \frac{s_3 - s}{s}, \right. \\ &\quad (M_K^2 - M_\pi^2) \frac{s_2 - s_1}{s}, \frac{(s - s_3)^2}{s^2} \left[(M_K^2 - M_\pi^2)^2 + \frac{\lambda}{3} \right], \\ &\quad \frac{(s_1 - s_2)^2}{s^2} \left[(M_K^2 - M_\pi^2)^2 + \frac{\lambda}{3} \right] + \frac{4\lambda}{3s} (s_3 - 4m^2), \\ &\quad \left. \frac{s_1 - s_2}{s^2} \left[(M_K^2 - M_\pi^2)^2 (s - s_3) - \frac{\lambda}{3} (s + s_3) \right] \right\}. \end{aligned} \quad (\text{C.6})$$

Putting pieces together, we find

$$\Omega_{\ell^+ \ell^-}^{\text{brems}} = \frac{\alpha}{\pi \sigma} \left\{ \frac{s - 2m^2}{s} I_2 - 2I_1 - 2I_3 + \frac{s I_4}{s + 2m^2} \right\}, \quad (\text{C.7})$$

where

$$\begin{aligned} I_1 &= \frac{m^2}{s} \int \frac{ds_1 ds_2}{(s_1 - m^2)^2}, \quad I_2 = \int \frac{ds_1 ds_2}{(s_1 - m^2)(s_2 - m^2)}, \\ I_3 &= \frac{1}{s} \int \frac{ds_1 ds_2}{s_1 - m^2}, \quad I_4 = \frac{1}{s^2} \int ds_1 ds_2 \frac{s_2 - m^2}{s_1 - m^2}. \end{aligned} \quad (\text{C.8})$$

Note that the integrals I_{1-4} are symmetric under the exchange $s_1 \leftrightarrow s_2$. We document the individual results for I_{1-4} for the most interesting cuts for $K \rightarrow \pi e^+ e^- \gamma$, in (or close to) the massless limit, corresponding to the full corrections factors in Eqs. (14), (16), and (17). In all cases, we show the “hard” parts of the integrals, i.e. those that, in the combination Eq. (C.7), have to be *subtracted* from the fully inclusive correction factor $\Omega_{e^+ e^-} = \alpha/4\pi + \mathcal{O}(m)$.

With a cut only on the photon energy, we find

$$\begin{aligned} I_1^{\text{hard}} &= -1 + \epsilon - \log \epsilon + \mathcal{O}(\delta), \\ I_2^{\text{hard}} &= 2 \text{Li}(\epsilon) - \frac{\pi^2}{3} + 2 \log \delta \log \epsilon + \mathcal{O}(\delta), \\ I_3^{\text{hard}} &= -(1 - \epsilon) [1 + \log \delta - \log(1 - \epsilon)] + \mathcal{O}(\delta), \\ I_4^{\text{hard}} &= -\frac{1 - \epsilon}{2} \left[\frac{5 + 3\epsilon}{2} + (1 + \epsilon) (\log \delta - \log(1 - \epsilon)) \right] \\ &\quad + \mathcal{O}(\delta), \end{aligned} \quad (\text{C.9})$$

with $\epsilon = 2E_{\text{max}}/\sqrt{s}$ and $\delta = m^2/s$ as in the main text. Imposing an additional cut on $\cos \theta_{e^\pm \gamma} = c_{e\gamma}$, we find in the massless limit $m = 0$

$$\begin{aligned} I_1^{e\gamma} &= 0, \quad I_2^{e\gamma} = 2 \log \epsilon \log \frac{1 - c_{e\gamma}}{1 + c_{e\gamma}} + \frac{\pi^2}{3} - 2 \text{Li}(\epsilon), \\ I_3^{e\gamma} &= (1 - \epsilon) \left[1 - \log(1 - \epsilon) - \log \frac{1 - c_{e\gamma}}{1 + c_{e\gamma}} \right], \\ I_4^{e\gamma} &= -\frac{1 - \epsilon}{2} \left[\frac{3}{2} (1 - \epsilon) + \frac{8}{1 - c_{e\gamma}} \right. \\ &\quad \times \left(\frac{1 + c_{e\gamma}}{(1 - c_{e\gamma})(1 - \epsilon)} \log \left(\epsilon + \frac{2(1 - \epsilon)}{1 + c_{e\gamma}} \right) - 1 \right) \\ &\quad \left. + (1 + \epsilon) \left(\log(1 - \epsilon) + \log \frac{1 - c_{e\gamma}}{1 + c_{e\gamma}} \right) \right]. \end{aligned} \quad (\text{C.10})$$

Finally, employing a cut on $\cos \theta_{e^+ e^-} = c_{ee}$, the hard, non-singular part of the bremsstrahlung integrals in the massless limit $m = 0$ is

$$\begin{aligned} I_1^{ee} &= 0, \quad I_2^{ee} = -\text{Li} \left(\frac{c_{ee} - 1}{c_{ee} + 1} \right), \\ I_3^{ee} &= -\frac{2}{1 - c_{ee}} \log \frac{1 + c_{ee}}{2} - 1, \\ I_4^{ee} &= \frac{1}{1 - c_{ee}} \left[\frac{2c_{ee}}{1 - c_{ee}} \log \frac{1 + c_{ee}}{2} + \frac{1 + 3c_{ee}}{4} \right]. \end{aligned} \quad (\text{C.11})$$

For completeness, we also add the equivalent of Eq. (C.5) for the $P \rightarrow V \ell^+ \ell^-$ and $V \rightarrow P \ell^+ \ell^-$ decays discussed in Sect. 5. The bremsstrahlung contribution to the correction factor can be written in the same form as Eq. (C.4) with $N_i \rightarrow N'_i$, $i = 1, 2, 3$, $\lambda \doteq \lambda(M_A^2, s, M_B^2)$,

$$\begin{aligned} N'_1 &= -4 \left\{ m^2 \left[\left(1 + \frac{4m^2}{s} \right) \lambda + \nu_1^2 \right] \right. \\ &\quad \left. + (s_1 - m^2) (M_A^2 - M_B^2) \nu_2 \right\}, \\ N'_2 &= -4 \left\{ m^2 \left[\left(1 + \frac{4m^2}{s} \right) \lambda + \nu_2^2 \right] \right. \\ &\quad \left. - (s_2 - m^2) (M_A^2 - M_B^2) \nu_1 \right\}, \\ N'_3 &= 4 \left\{ (s_3 - 2m^2) \left(1 + \frac{4m^2}{s} \right) \lambda + \frac{s}{2} (\nu_1^2 + \nu_2^2) \right. \\ &\quad \left. - 2m^2 \nu_1 \nu_2 + \frac{1}{2s} \left[\lambda + (M_A^2 - M_B^2)^2 \right] \right. \\ &\quad \left. \times \left[(s_1 - m^2)^2 + (s_2 - m^2)^2 \right] \right\}. \end{aligned} \quad (\text{C.12})$$

The angular integration Eq. (C.6) holds as before with the replacements $M_K \rightarrow M_A$, $M_\pi \rightarrow M_B$. As already pointed out in Sect. 5, the result Eqs. (C.7) and (C.8) are then reproduced identically as in the decay $K \rightarrow \pi \ell^+ \ell^-$.

References

1. G. Ecker, A. Pich and E. de Rafael, Nucl. Phys. B **291**, 692 (1987).
2. G. D’Ambrosio, G. Ecker, G. Isidori and J. Portolés, JHEP **9808**, 004 (1998) [arXiv:hep-ph/9808289].
3. S. Friot, D. Greynat and E. de Rafael, Phys. Lett. B **595**, 301 (2004) [arXiv:hep-ph/0404136].
4. J. Bijnens and K. Ghorbani, arXiv:0711.0148 [hep-ph].
5. P. Bloch *et al.*, Phys. Lett. B **56**, 201 (1975).
6. C. Alliegro *et al.*, Phys. Rev. Lett. **68**, 278 (1992).
7. R. Appel *et al.* [E865 Collaboration], Phys. Rev. Lett. **83**, 4482 (1999) [arXiv:hep-ex/9907045].
8. J. R. Batley *et al.* [NA48/2 Collaboration], Phys. Lett. B **677**, 246 (2009) [arXiv:0903.3130 [hep-ex]].
9. S. C. Adler *et al.* [E787 Collaboration], Phys. Rev. Lett. **79**, 4756 (1997) [arXiv:hep-ex/9708012].
10. H. Ma *et al.* [E865 Collaboration], Phys. Rev. Lett. **84**, 2580 (2000) [arXiv:hep-ex/9910047].
11. H. K. Park *et al.* [HyperCP Collaboration], Phys. Rev. Lett. **88**, 111801 (2002) [arXiv:hep-ex/0110033].
12. E. Goudzovski, PoS **KAON09**, 009 (2009) [arXiv:0908.3860 [hep-ex]].
13. J. R. Batley *et al.* [NA48/1 Collaboration], Phys. Lett. B **576**, 43 (2003) [arXiv:hep-ex/0309075].
14. J. R. Batley *et al.* [NA48/1 Collaboration], Phys. Lett. B **599**, 197 (2004) [arXiv:hep-ex/0409011].
15. G. Isidori, Eur. Phys. J. C **53**, 567 (2008) [arXiv:0709.2439 [hep-ph]].
16. F. Bloch and A. Nordsieck, Phys. Rev. **52**, 54 (1937).
17. D. R. Yennie, S. C. Frautschi and H. Suura, Annals Phys. **13**, 379 (1961).
18. S. Weinberg, Phys. Rev. **140**, B516 (1965).
19. G. Gamow, Z. Phys. **51**, 204 (1928).
20. A. Sommerfeld, *Atombau und Spektrallinien*, vol. 2, Vieweg, Braunschweig (1939).
21. M. Bissegger, A. Fuhrer, J. Gasser, B. Kubis and A. Rusetsky, Nucl. Phys. B **806**, 178 (2009) [arXiv:0807.0515 [hep-ph]].
22. J. Gasser, B. Kubis, N. Paver and M. Verbeni, Eur. Phys. J. C **40**, 205 (2005) [arXiv:hep-ph/0412130].
23. B. Kubis, E. H. Müller, J. Gasser and M. Schmid, Eur. Phys. J. C **50**, 557 (2007) [arXiv:hep-ph/0611366].
24. G. Bell, J. H. Kühn and J. Rittinger, arXiv:1004.4117 [hep-ph].
25. T. Kinoshita, J. Math. Phys. **3**, 650 (1962).
26. T. D. Lee and M. Nauenberg, Phys. Rev. **133**, B1549 (1964).
27. K. Kampf, M. Knecht and J. Novotný, Eur. Phys. J. C **46**, 191 (2006) [arXiv:hep-ph/0510021].
28. J. Bijnens, A. Bramon and F. Cornet, Phys. Rev. Lett. **61**, 1453 (1988).
29. C. Terschläusen and S. Leupold, Phys. Lett. B **691**, 191 (2010) [arXiv:1003.1030 [hep-ph]].